ELSEVIER

Ceramics International 28 (2002) 451–458

CERAMICS INTERNATIONAL

www.elsevier.com/locate/ceramint

Structural and electrical properties of zirconia/hydroxyapatite porous composites

M. Sh. Khalil[a], Hanan H. Beheri[b], Wafa I. Abdel Fattah[b,*]

[a]*Inorganic Chemistry, National Research Centre, Tahrir St., Dokki, Cairo, Egypt*
[b]*Ceramics Department, National Research Centre, Tahrir St., Dokki, Cairo, Egypt*

Received 15 May 2001; received in revised form 31 August 2001; accepted 3 October 2001

Abstract

Zirconia/hydroxyapatite porous composites containing 7.58–32.89% ZrO_2 were sintered at 1000 and 1250 °C. Relative porosity (ΔP) decreases with increased ZrO_2 content at both firing temperatures. Sintering at 1250 °C, however, was accompanied by higher ΔP as a consequence of a partial transformation of HA (hydroxyapatite) to β-TCP (β-tricalcium phosphate) besides partial stabilization of the ZrO_2 tetragonal phase. The higher ZrO_2 content and/or sintering temperature resulted in reduced a-axis of HA and increased its c-axis. On the other hand, a reduction of both a- and c-axes is recorded in the formed β-TCP denoting cell contraction with higher ZrO_2 content and sintering at 1250 °C. Scanning electron microscopy (SEM) showed the presence of HA and ZrO_2 in the composite sintered at 1000 °C. The transformation of monoclinic ZrO_2 to the tetragonal phase and HA to β-TCP at 1250 °C was assured. The dielectric constant ε' and loss ε'' values were minimum at low measuring temperatures (298–593 K) and low frequencies (frequency range 10^2–1×10^6 HZ). Multiple relaxation peaks and frequency shifts in conductivity/ frequency relations were related to zirconia content, elimination of CO_3^{2-} and porosity as well as multiple phase achieved at high sintering temperature.

Keywords: C. Electrical properties; Structure; ZrO_2/HA; Porous composites

1. Introduction

Recent applications of Ca-apatites, besides their unique role as biocompatible bioactive bioceramics [1], are their functions in electric devices such as sensors for humidity, carbon dioxide and alcoholic gases [2]. Zirconia can be used clinically as it retains bending strength when introduced in the medullary cavity of rabbits tibia up to 3 years [3]. Also tetragonal polycrystalline zirconia was reported as a high performance solid oxygen ion conductor [4]. Both fields of applications necessitate the assessment of structural features including porosities as well as electrical and dielectric properties. Previous work on monoclinic zirconia/hydroxyapatite composites dealt with their preparation and in vitro degradation in human serum in relation to phase assembly [5]. Literature pertaining to bioelectric compatibility of materials is very rare. Natural bone manifests a particular electrical pattern which is believed to have an important influence on the architecture, composition and physiology of living bone [6,7].

The present work focuses on microstructural and electrical properties of porous zirconia/HA composites in comparison with HA.

2. Experimental procedure

2.1. Apatite composites

Five powder samples were prepared from (Ca-AP) calcined bovine hydroxyapatite (B) and monoclinic zirconia. Details of sintering conditions and ceramic parameters were given elsewhere [8].

2.2. Structural assessment

2.2.1. Crystalline structure

X-ray diffraction analysis was performed to identify phases and calculate lattice parameters (least-square method) using diffraction peaks at (212), (312), (213),

* Corresponding author.

0272-8842/02/$22.00
PII: S0272-8842(01)00118-3

(410), (004) and (502) for HA and (006), (300) (202) (104) (214) for β-TCP. Philips X-ray diffractometer (1060/70) was operated at $2\theta = 0.2°$/min and Cu K_α radiation.

2.2.2. Microstructure

The variation in microstructure of the Ca-AP and Zr/Ca-Ap composites as a function of sintering temperature and ZrO_2 content was examined using SEM (Jeol-TSU-TZ and 19 Kev, Japan). X-ray unit attachment (EDAX) was used to compare the intensities of calcium (Ca), phosphor (P) and zirconium (Zr). Samples were diamond polished, thermally etched (to avoid monoclinic content at the surface) and sonicated in alcohol. The composites, dried in acetone and sputtered with gold, were mounted on a copper holder with golden coating as an adhesive and electric conductor.

2.3. Electrical properties

Measurements of electrical conductivity (σ_{ac}) were carried out as a function of temperature (298–593 K) using the ac two probe method. LCR oscillator (Hioki 42 Hz–5 MHz, Japan) was adjusted at 50 kHz. Platinum electrodes were attached to the samples and connected to the LCR. Dielectric constant (ε') and dielectric loss (ε'') measurements were carried out between 298 and 593 K in the frequency range (100 Hz–1 MHz) using the same instrument.

3. Results and discussion

3.1. Structural assessment

3.1.1. Porosity development

The results of relative porosity (ΔP) of Zr/Ca-AP composites ($\Delta P = P_{zrAP}\text{-}P_{CaAP}/P_{CaAP}$) sintered at 1000 and 1250 °C show a similar trend of descending values at increased zirconia content. Compacts with the highest contents of zirconia Z_3/Ca-AP and Z_4/Ca-AP (Table 1) sintered at 1250 °C, have higher values compared with those sintered at 1000 °C (Fig. 1). This is due to the HA→ β-TCP transformation [9] and t↔m martensitic transformation of ZrO_2 [4].

3.1.2. Crystalline structure

On sintering at 1000 °C, the persistence of HA structure in Ca-Ap sample and composites with 7.58 or 17.0% ZrO_2 was evidenced. Higher amounts of ZrO_2 assisted HA transformation to β-TCP partially reduced a-axis and enlarged c-axis of HA. Composites with ZrO_2 higher than 17% revealed the presence of monoclinic ZrO_2 and $CaZr_4O_9$ at dÅ = 2.97,2.57 and 1.82 (Fig. 2). Sintering at 1250 °C, maintained HA structure of the base sample. Addition of 7.58% zirconia did not

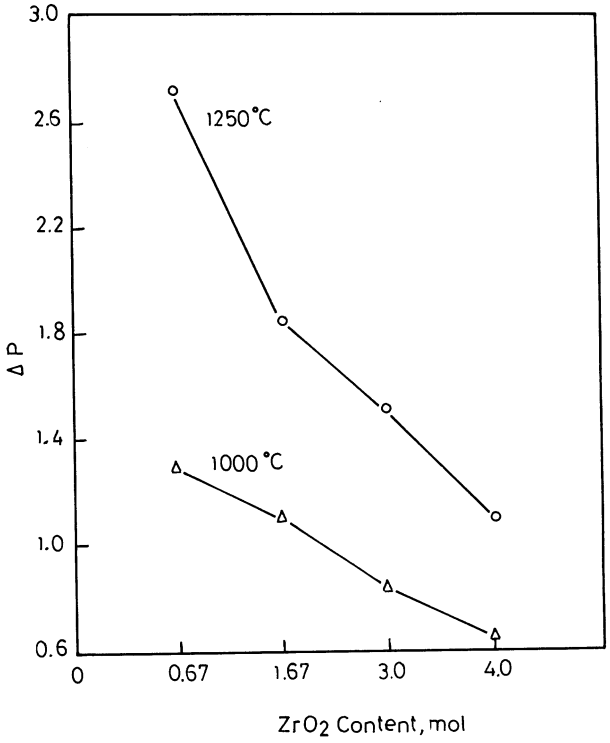

Fig. 1. Relative porosity (ΔP) of a Ca-Ap sample and Zr/Ca-Ap composites sintered at 1000 and 1250 °C.

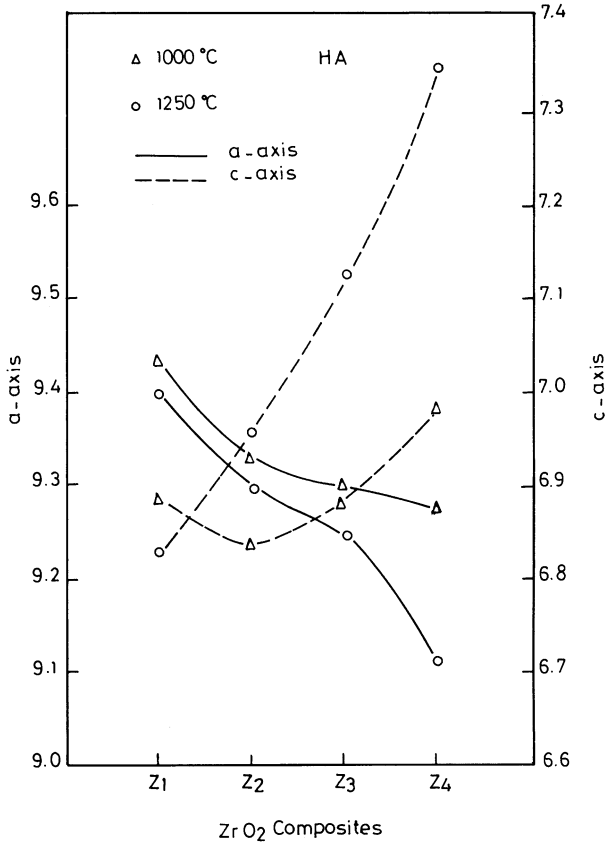

Fig. 2. Lattice parameters of HA in Ca-Ap sample and Zr/Ca-Ap composites sintered at 1000 and 1250 °C.

affect phase changes while higher contents of ZrO_2 resulted in β-TCP as a predominant phase along with m-ZrO_2. The tetragonal ZrO_2 phase was also detected (dÅ = 2.96, 1.83 and 1.55). This is in agreement with the work done by Nagaraja and Rao [9] on HIP samples.

The transformation of HA to β-TCP affected the values of relative porosity ΔP where the applied heating energy was consumed in phase transformation rather than assisting the sintering process. Malagon et al. [10] reported that reactive sintering at 1150 °C for 7 days with 30–40% ZrO_2, lowered the decomposition temperature of HA to β-TCP and enhanced α-TCP formation. In the present work no signs of α-TCP were detected.

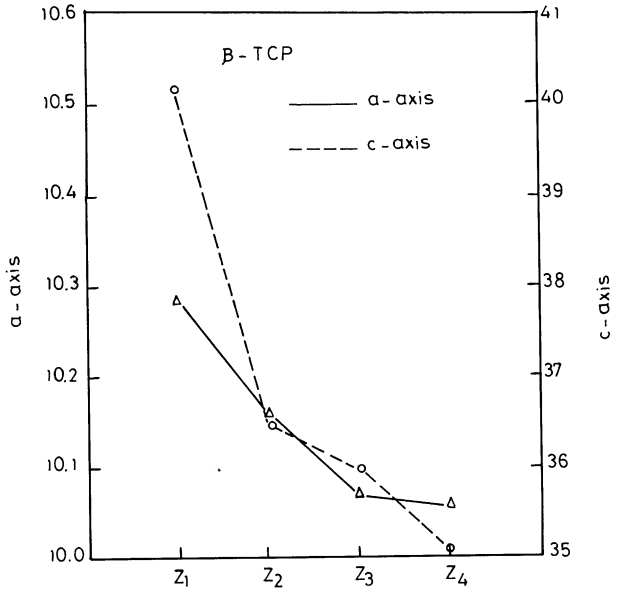

Fig. 3. Lattice parameters of β-TCP in Zr/Ca-Ap composites sintered at 1250 °C as a function of zirconia content.

The Ca-Ap sample (1000 °C) possessed lattice parameters specific for HA which were enlarged on higher firing temperature (1250 °C) i.e. cell growth. Reduced a-axis and increased c-axis of HA, in parallel with ZrO_2 content higher than 7.58%, were achieved. Higher firing temperature (1250 °C) enhanced the same trend. Such phenomena were related to dehydroxylation and transformation to oxyhydroxyapatite [5]. However, since these cell variations were observed in the presence of ZrO_2, and as previous IR data assured the persistence of HA up to 1250 °C [5], the present variations are related to the elimination of CO_3^{2-} groups structurally present in Ca-Ap. The β-TCP phase suffered higher cell contraction in parallel with higher ZrO_2 content (Fig. 3).

3.1.3. Microstructure

3.1.3.1. Sintering at 1000 °C. Ca-Ap sample possessed clusters of aggregated HA scales entrapping pores at the junction of three or more grains [Fig. 4(a)]. Such clusters are due to Van der Waals forces and are inherent to the present dry-powder consolidation route. Spheroid grains of high optical density (0.5 and 1 μm) are homogenously

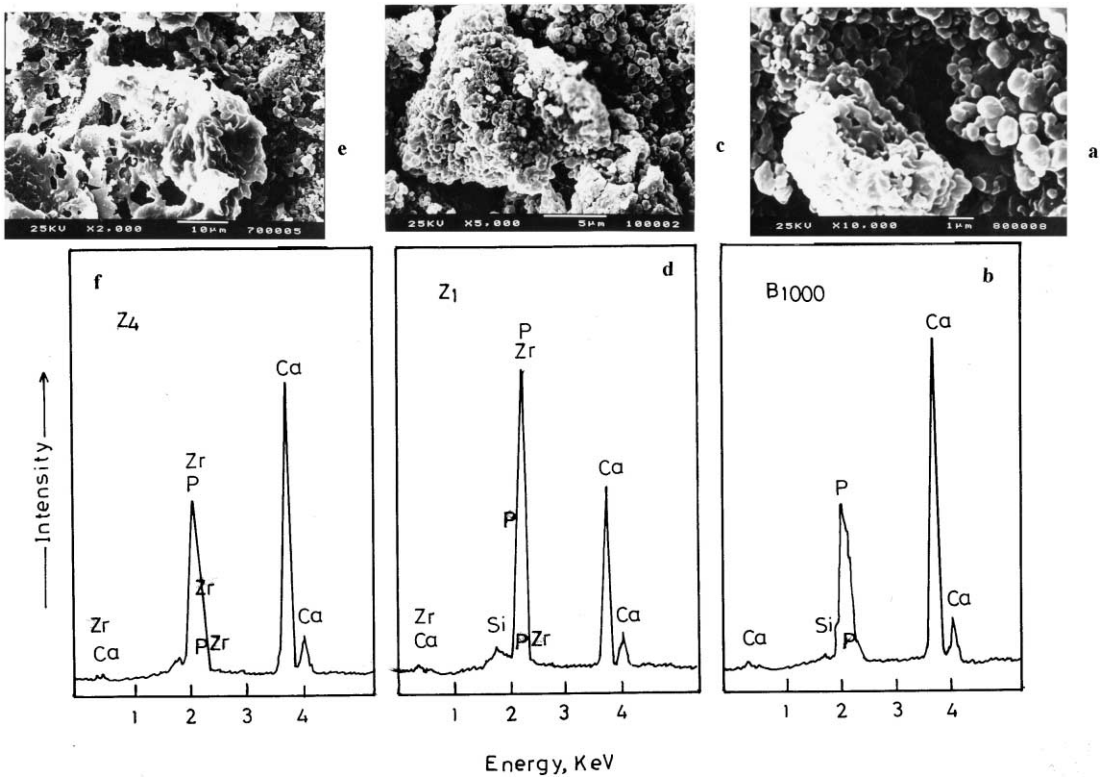

Fig. 4. Microstructural features (SEM) of thermally etched Ca-Ap sample and Zr/Ca-AP composites sintered at 1000 °C with their EDAX.

distributed. Fusion of grain boundaries is clear within the cluster area. The Ca/P ratio of their elemental analysis is typical for HA [Fig. 4(b)] [11]. In the presence of 7.58 wt.% ZrO_2 large clusters of HA scales were observed along with few opaque grains of ZrO_2 below 1 μm [Fig. 4(c)]. Its EDAX spectrum [Fig. 4(d)] revealed equal proportions of Zr and P at the expense of Ca. Negligible variations could be detected in the morphologies of composites with higher ZrO_2 content. The micrograph of the Z_4/Ca-Ap composite revealed an advanced sintering stage coinciding with $\Delta P = 0.63$. A large cluster of aggregated HA with fused grain boundaries entrap closed pores having square and penny shapes [Fig. 4(e)]. The relatively reduced Ca peaks in the EDAX spectrum [Fig. 4(f)] complement the leaching of calcium and its dissolution to stabilize tetragonal ZrO_2 and/or form Ca-zirconate phases following transformation of HA to β-TCP.

3.1.3.2. Sintering at 1250 °C. Ca-Ap sample possessed a fused groundmass retaining relicts of grain boundaries (dark portion) [Fig. 5(a)]. Within the HA clusters, several neck areas at the junction of two or more spheroidal HA grains showed remarkable grain growth (1.2–2.5 μm) proving advanced stage of sintering (91% theoretical

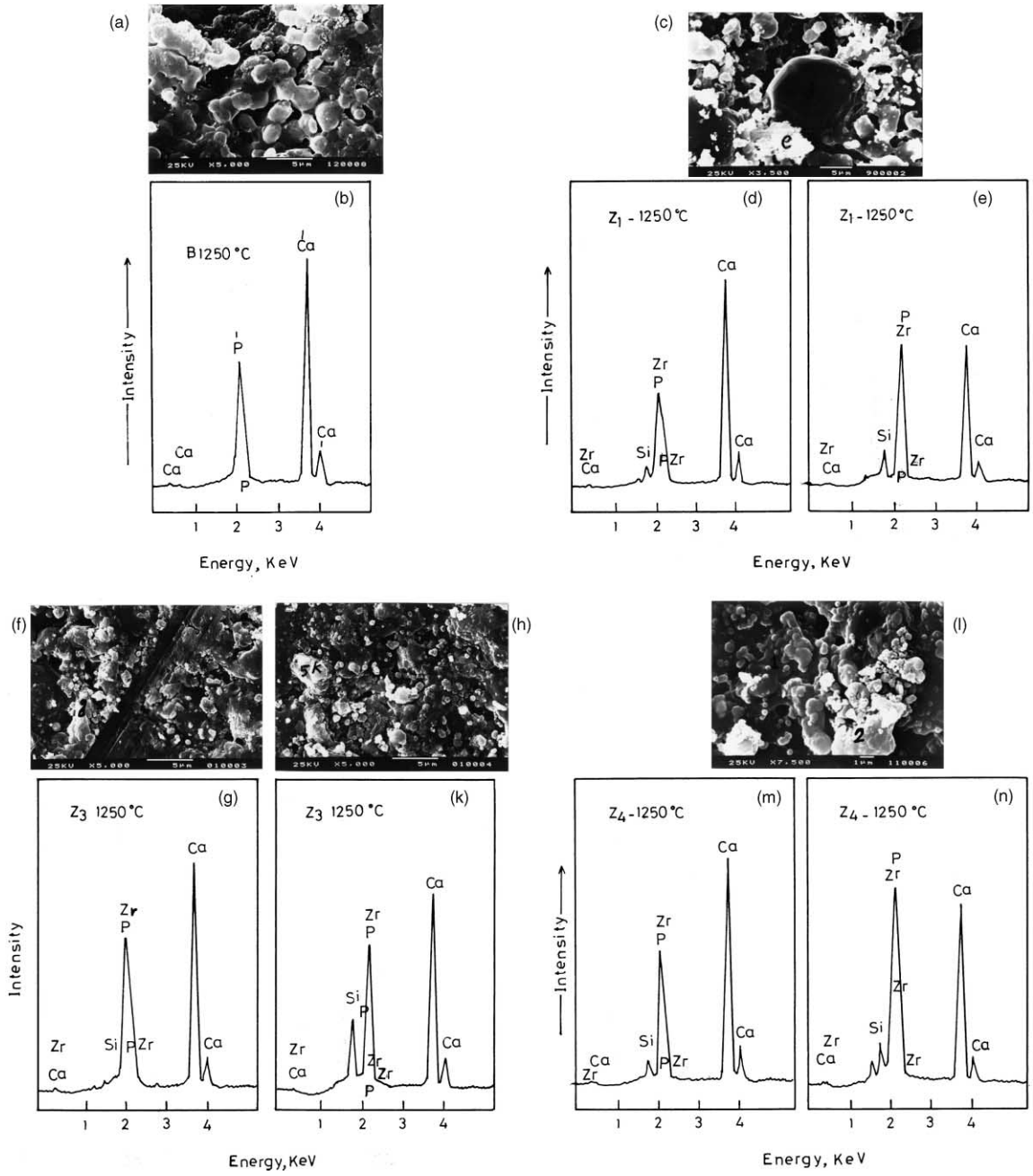

Fig. 5. Microstrucural features (SEM) of a thermally etched Ca-AP sample and Zr/Ca-Ap composites sintered at 1250 °C with their EDAX.

density). A significant portion of the pore channels had collapsed to isolated pores. The coincidence of the transition in grain growth behaviour with the collapse of pore channels to isolated pores agrees with the idea of grain growth limited by pores mobility. The local curvature of the developing neck region between particles hinders the motion of the grain boundaries during the sintering process. For the boundary to leave the neck region it requires an increase in the free energy of the system as a direct result of an increase in boundary area. The neck region particles of low coordination can be eliminated by transport mechanisms such as surface diffusion which do not directly contribute to densification. If the pores are formed by several particles, surface diffusion leads only to spherodization of the interparticle voids, rather than the elimination of local curvature. The EDAX spectrum [Fig. 5(b)] typically records the peaks of Ca and P with HA ratio proving its persistence and complement XRD data. Composites with 7.5% ZrO_2 possessed uniquely rounded exaggerated grain growth (14 μm) related to $CaZr_4O_9$ calcium zirconate phase which is superimposed on the aggregates of HA scales [Fig. 5(c)]. Fused elongated grains with several neck areas form the groundmass with elliptic pore shapes. Particles and/or pore size variation within the compact can cause large particles to grow at the expense of smaller ones. The variation in particle coordination number can lead to differential sintering. High particle coordination i.e. dense agglomerates sinter to the closed pore state earlier than loosely packed regions. This causes inhomogeneous grain growth so that some regions of the porous body has a large grain size while the surrounding regions still contain interconnected porosity. Grain growth may increase even though the sintering behaviour is predominantly in the intermediate stage ($\Delta P = 2.45$). The coincidence of the transition in grain growth behaviour with the collapse of pore channels to isolated pores agrees with the idea of grain growth limited by pores mobility. Dark exaggerated grains have combined peaks of Ca, Zr and P atoms [Fig. 5(d)]. The EDAX spectrum of the light scales recorded Ca, P and Zr but with relatively lower intensities [Fig. 5(e)]. A negligible difference could be observed for the Z_2/Ca-Ap composite (17% ZrO_2). A higher concentration of ZrO_2 i.e. Z_3/Ca-Ap, resulted in a massive structure and longitudinal parallel alignment (dark portions) crossing the field. Several morphologies of HA and β-TCP were observed within the original cluster of HA grains [Fig. 5(f)]. The EDAX spectrum of the dark portion proved its enrichment in Ca,P and Zr elements. The light portion [Fig. 5(g)] revealed a lower Ca content comparatively. A characteristic groundmass of dark fused grains retaining the pores between the grains and grain boundaries were observed in another area [Fig. 5(k)]. Several spheroidal light and dark grains probably t-and m-ZrO_2 (0.7, 1, 1 and 2 μm) were homogenously spread all over the field. The rounded morphology of the grains is believed to be a consequence of the presence of a liquid phase during sintering. The photomicrographs of the Z_4/Ca-Ap composite revealed two distinct phases of fused aggregates of HA scales (light portion) with relicts of grain boundaries [Fig. 5(l)]. An advanced stage of sintering ($\Delta P = 1.14$) is proved by the development of several neck areas between the particles and the penny shaped pores (1 μm or less) trapped within the groundmass. Typical rounded grains (0.5 μm size) are probably Ca-stabilized t-ZrO_2. Highest ZrO_2 seems to impede the grain growth of HA. Two habits of phases are recorded: one is a non crystalline liquid phase produced during sintering with a smooth surface (site 1) and the other is an interlocking structure of plate like crystals (site 2). The EDAX spectrum of the agglomerated portion is characterized by enhanced intensity of the Ca peak and lower peaks of P and Zr [Fig. 5(n)]. This is consistent with those recorded with a composite of lower ZrO_2 and suggests that the growing crystal phases are composed of a combination of different crystal components. The EDAX of the dark area [Fig. 5(o)] proved there were equal proportions of Ca/P and Zr peaks.

3.2. Electrical properties

3.2.1. Conductivity

The Arrhenius plots of electrical conductivity (σ) of Ca-AP and Ca-AP substituted ZrO_2 composites sintered at 1000 °C [Fig. 6(a)] and 1250 °C [Fig. 6(b)] showed increased values with higher measuring temperature. Substitution by Zr^{4+} affected the change of charge carrier and conduction mechanism. Kijima et al. [12] reported that electrical conduction in Ca-AP is achieved by hydroxyl ions migration through vacancies (produced by sintering) in the center of calcium ion triangle planes along the c-axis of the hexagonal structure. The transport of OH^- vacancies along the c-axis enhanced the conduction mechanism in the electrical properties of Ca-AP. Maiti et al. [13] recorded that protonic conduction in fluoro-HAP was due to proton hopping between adjacent oxygen (O^{2-}) and hydroxyl (OH^-) ions in substituted (-Y^-)-AP. Change of σ with increasing substituted Zr^{4+} ions might be explained by the decrease of charge- carrying proton density due to O^{2-} and OH^- .

Table 1
Compositions of the zirconia/apatite composites

Oxides	Notation				
	Ca-Ap (B)	Z_1/Ca-AP	Z_2/Ca-Ap	Z_3/Ca- Ap	Z_4/Ca-AP
			Wt.%		
ZrO_2	–	7.58	17.01	26.87	32.09
CaO	56.79	51.55	46.29	40.79	37.43
P_2O_5	43.21	39.25	35.21	31.03	28.48

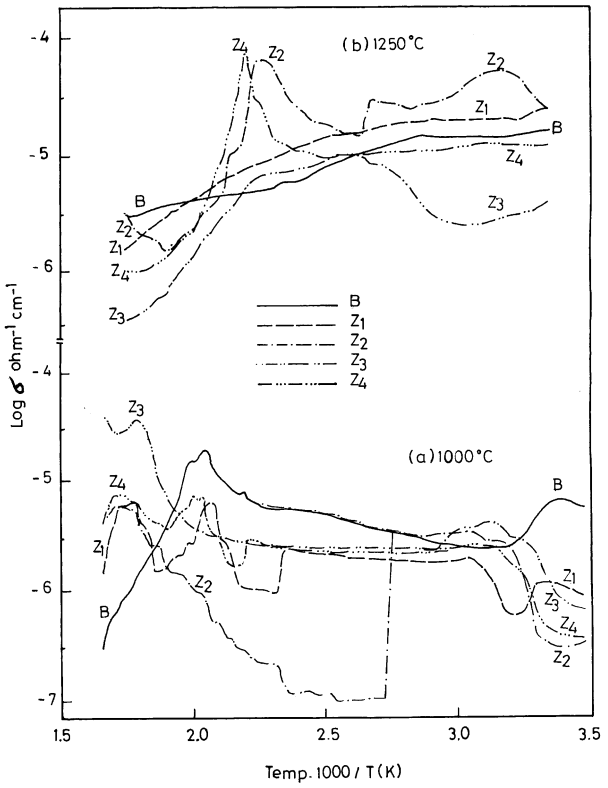

Fig. 6. Arrhenius plots log σ vs 1000/K of Ca-Ap sample and Zr/Ca-Ap composites sintered at 1000 and 1250 °C.

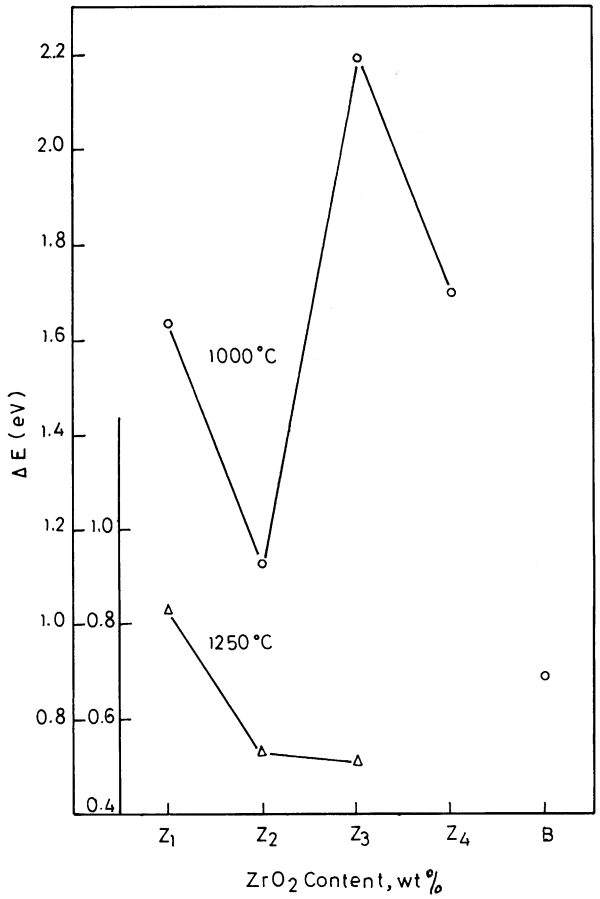

Fig. 7. Activation energies of a Ca-Ap sample and ZrO_2 content replacing HA.

Segregates of a small amount of highly resistive ZrO_2 at the intergranular spacings in the ceramic matrices would reduce the total conductivity. Temperature independent regions were observed in the low measuring temperature of the Arrhenius plots, whose length varied according to ZrO_2 content.

This was explained as frozen equilibrium between the concentration of defects and charge carriers with the measuring temperature.

Activation energy values ΔE (eV), calculated from Arrhenius plots within the ascending portion of the curves in the temperature dependent region, were plotted as a function of ZrO_2 content replacing HA (Fig. 7). On sintering at 1000 °C, the Ca-AP base sample recorded the lowest ΔE value (0.9 eV). In the presence of Zr^{4+}, ΔE values are doubled and follow the order Z_3 / Ca-AP > Z_4 /Ca-AP > Z_1/Ca-AP > Z_2/Ca-AP, with 2.2, 1.70, 1.64 and 1.13 eV respectively. Activation energy values of samples sintered at 1250 °C gradually decreased in parallel with higher Zr^{4+} content but with a negligible difference between Z_2/and Z_3/Ca-Ap composites recording 0.54 and 0.51 eV, respectively. It was not possible to calculate ΔE values corresponding to the Ca-Ap sample or Z_4/Ca-Ap composite. Activation energies for O^{-2} and OH^- conduction in HA within a similar temperature range were recorded as 1.5 and 2.1 eV, respectively [2]. The present situation is different due to the multiphase nature of the samples containing ZrO_2, HA and porosity at low sintering temperature. Additional β-TCP, t-ZrO_2 m-ZrO_2, and $CaZr_4O_9$ phases with lower but existing porosity were recorded, leading to lower conductivity values at higher sintering temperature.

Variation of σ values versus frequency of the Ca-AP sample and Z_1-Ca-AP composites sintered at 1000 and 1250 °C is shown in Fig. 8. The nonlinear conductivity / frequency response at room temperature with multiple relaxation peaks is proved. Such an evolution corresponds to conductivity relaxation modes due to the coulomb interactions of the charge carriers and the disorder within the structure, suggesting a Maxwell–Wagner mechanism. This is consistent with similar trends in disordered solid porous calcite rocks and bone tissue [14]. Larger relaxation peaks and higher conductivity with higher sintering temperature in a Ca-AP base sample are consequences of disorder accompanying the elimination of CO_3^{2-} and the developed glassy phase. The presence of β-TCP with the transformation of ZrO_2 and a larger cell volume compared to HA would contribute to higher charge mobility. Interfacial polarization is expected, additionally, as dispersion occurs in the bulk properties from the charging of interfaces within the matrix.

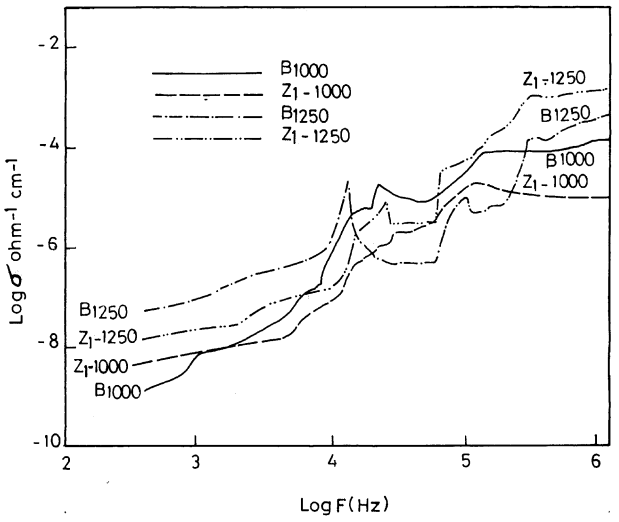

Fig. 8. Conductivity at room temperature at various frequencies of Ca-Ap and Z_1/Ca-Ap composite sintered at 1000 and 1250 °C.

3.2.2. Dielectric properties

The dielectric constant (ε') values vs log frequency [Fig. 9(a)] for samples sintered at 1000 °C showed substantial dielectric dispersion especially for the Ca-Ap sample and Z_1/Ca-AP composite with minimum ZrO_2 content. Higher ZrO_2 contents reduced the (ε') values according to the order Z_2 /Ca-AP < Z_4/Ca-AP < Z_3/Ca-AP. Dielectric absorption was not recorded behind 10^4 Hz. On sintering at 1250 °C [Fig. 9(b)] a similar trend but with lower values was observed. The lowest values of ε' followed the order Ca-AP < Z_2/Ca-AP = Z_1/ Ca-AP < Z_4/ Ca-AP. Therefore, the relaxation time and ionic species of dielectric polarization are greatly reduced by a higher sintering temperature and higher ZrO_2 content, resulting in lower porosity and more β-TCP phase beside the elimination of CO_3^{2-} ions and development of a Ca Zr_4O_9 phase [15].

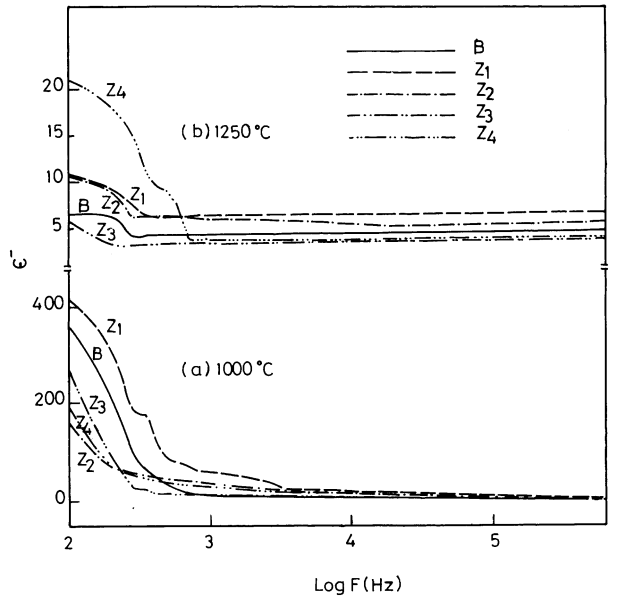

Fig. 9. Dielectric constant ε' values vs log frequency of a Ca- Ap sample and Zr/Ca-Ap composites sintered at (a) 1000 °C and (b) 1250 °C.

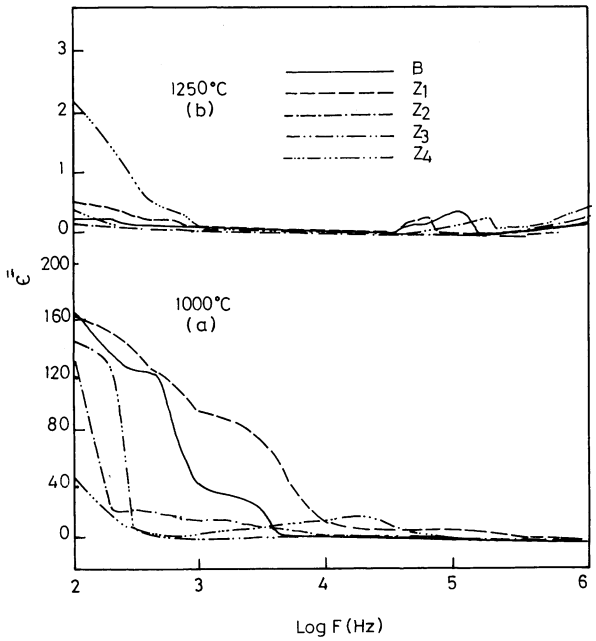

Fig. 10. Dielectric loss ε'' vs log frequency of a Ca-Ap sample and Zr / Ca-Ap composites sintered at (a) 1000 °C and (b) 1250 °C.

Dielectric loss (ε'') vs log frequency plots (Fig. 10) proved that dielectric absorption is reduced in parallel with increased ZrO_2 to be minimum for Z_4/Ca-AP, having a higher ZrO_2 content. Higher values of (ε'') at low frequencies for the Ca-Ap sample and Z_1/Ca-Ap composite with minimum ZrO_2 content were recorded when sintered at 1000 °C [Fig. 10(a)]. On sintering at 1250 °C, only the composite with maximum ZrO_2 content has the highest (ε'') [Fig. 10(b)]. The dielectric loss values were tremendously reduced by a factor of 160–140 except for the Z_4/Ca-AP composite which was reduced by factor of 20.

4. Conclusions

Lower sintering rates were related to the HA→β-TCP transformation and stabilization of the t-form of ZrO_2 by liberated Ca^{2+} which are affected by a ZrO_2 content higher than 7.58% especially on sintering at 1250 °C.

Reduced and enlarged a- and c-axes of HA, respectively, are accompanied by contraction of both axes of β-TCP with a higher ZrO_2 content and/or sintering temperature.

High rates of sintering of Ca-Ap scales were evidenced by a glassy phase, neck areas developed and entrapped closed pores. Differential grain growth and Ca-zirconate superimposed on HA scales showed limited solubility of ZrO_2 in the composites. Elemental analyses complemented the detected phases.

Composites containing 7.58% ZrO_2 possessed great similarity to the Ca-Ap base sample and the electrical properties are reduced with the inclusion of higher amounts of ZrO_2. Composite Z_3-HAP containing 26.87% ZrO_2 had minimum values.

High sintering temperature tremendously reduced the conductivity activation energy especially in the presence of high Zr^{4+} content.

The shift of conductivity relaxation peaks to a higher frequency was related to the developed glassy phase, β-TCP with a larger cell volume than HA and disorder accompanying carbonate elimination.

References

[1] L.L. Hench, Bioactive materials, the potential for tissue engineering, 24th Ann. Meeting, CA, 1998.
[2] K. Yamashita, H. Owada, H. Nakagawa, T. Umegaki, T. Kanazawa, J. Am. Ceram. Soc. 69 (8) (1986) 590.
[3] K. Shimizu, M. Oka, P. Kumar, Y. Kotoura, T. Yamamuro, K. Makinouchi, T. Nakamura, J. Biomed. Mater. Res. 27 (6) (1993) 929.
[4] W. Weppner, Solid State Ionics 1–3 (1995) 15.
[5] W.I. Abdel-Fattah, H.H. Beheri, New Biomedical Materials Basic and Applied Studies, Ios Press, Amsterdam, 1998, pp. 91–97.
[6] C.A.L. Basset, Clin. Orthop. (1965) 35.
[7] M.H. Shamos, L.S. Lavine, Clin. Orthop. (1964) 33.
[8] H.H. Beheri, The Preparation and Characterization of Composite Phosphate Bioceramic, PhD thesis, Cairo University, 1999.
[9] V.S. Nagarajan, K.J. Rao, J. Mater. Chem. 3 (1993) 43–51.
[10] G.P. Malagon, S.J.P. Val Dés, G.G. Gosgas, J.O. López, E. Diaz, 4th Euro Ceramics 8 (1995) 1183–1777.
[11] P.T. Cheng, P.H. Protzkev, Calc. Tissue Int. 35 (1983) 596–601.
[12] T. Kijima, M. Tsutsumi, J. Am. Ceram. Soc. 62 (1979) 455–460.
[13] G.C. Maiti, F. Freund, J. Chem. Soc. Dalton Trans. (1981) 949–955.
[14] K. R. Foster, H. P. Schwan, Handbook of Biological Effects of Electromagnetic Fields, Shapter CRC press, 1996.
[15] A. Bensoud, M. El-Azzouzi, A. Bouhaouss, M. Ferhat, Phos. Res. Bull. 10 (1999) 2894.